

Supporting Information

Activated carbon versus montmorillonite embedded on porous chitosan beads for the treatment of olive mill wastewater: A comparative study

Wahid Ben Khadda,^a Oumaima Bahammou,^b Farah El Hassani,^a Nadia Katir,^a
Hicham Zaitan,^b Abdelkrim El Kadib.^{a,c,*}

^a *Euromed University of Fes, UEMF, Morocco a.elkadib@ueuromed.org*

^b *Processes, Materials and Environment Laboratory (LPME), Faculty of Sciences and Technology of Fez, Sidi Mohamed Ben Abdellah University, B.P. 2202 Fez, Morocco.*

^c *Hassan II Academy of Science and Technology, Rabat, Morocco*

Contents

Figure S1. Multistep preparation of Calcium-alginate hydrogel beads.

Figure S2. Adsorption kinetics of syringic acid using chitosan beads and calcium alginate beads.

Figure S3. Photographs of chitosan and calcium–alginate hydrogel beads before and after adsorption of syringic acid

Figure S4. FTIR spectra of chitosan hydrogel beads before and after syringic adsorption.

Figure S5. Adsorption kinetics and performance after 3 h and 24 h of contact of chitosan and chitosan-filled beads toward syringic acid.

Figure S6. Schematic illustration of the structural arrangements of layered nanosheets within polymer matrices as a function of the filler content: agglomeration, intercalation and exfoliation.

Table S1. Textural properties of the investigated materials.

Figure S6. Top. CS-MMT a) before and after caffeic acid adsorption and b) before and after syringic acid adsorption. Bottom. CS-AC a) before and after caffeic acid adsorption and b) before and after syringic acid adsorption.

Figure S7. SEM of activated carbon (AC) and montmorillonite (MMT)

Table S2. Residual mass (%) of adsorbents at selected temperatures from TGA analysis.

Figure S8. Comparative Views of **CS@MMT_50:50_HB** and **CS@AC_50:50_HB** Beads Before and After Adsorption of Caffeic and Syringic Acids

Figure S9. DRFIT spectra of **CS@AC_50:50_HB** before and after adsorption of syringic acid and caffeic acid.

Table S3. Physicochemical parameters of raw, diluted, and treated Olive Mill Wastewater (OMW) using chitosan-filled beads

Figure S10. Adsorption performance of OMW-saturated chitosan and chitosan-filled beads Toward Congo Red, Tetracycline, and Copper(II) Ions

Figure S1. Multistep preparation of Calcium-alginate hydrogel beads.

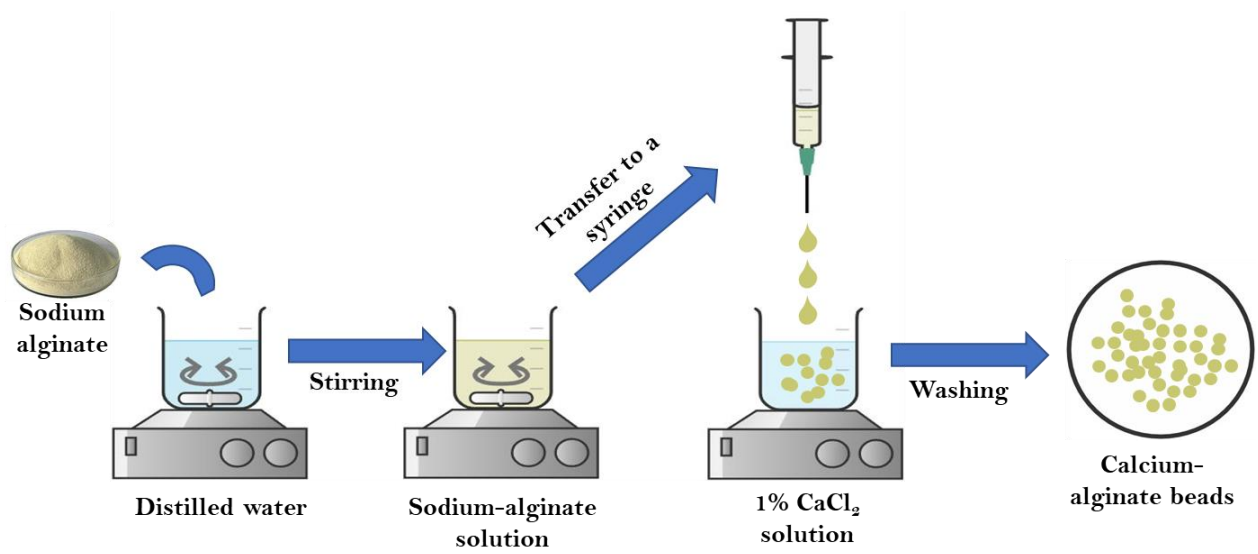


Figure S2. Adsorption kinetics of syringic acid using chitosan beads and calcium alginate beads.

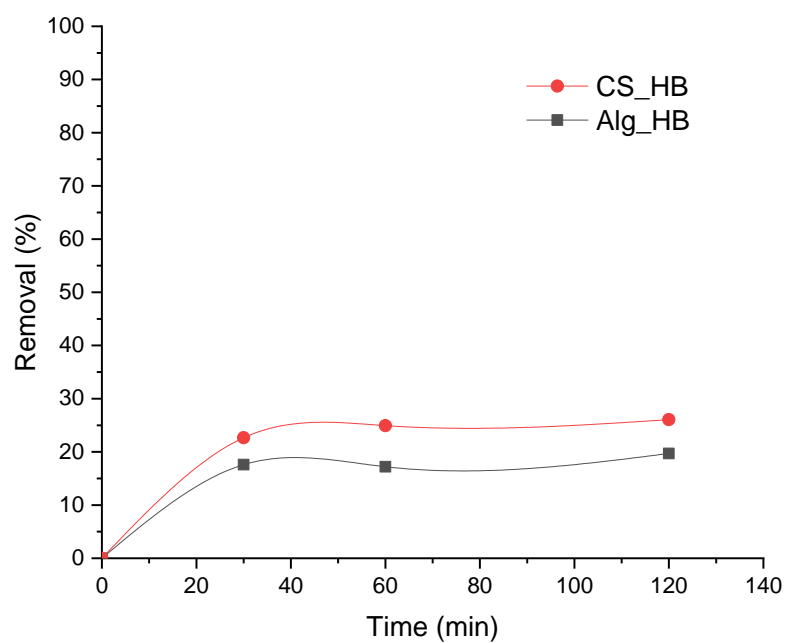
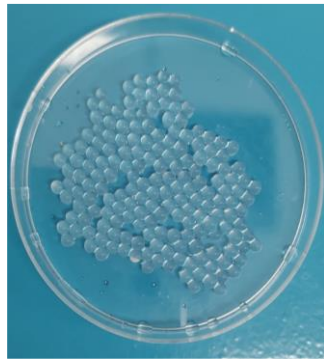
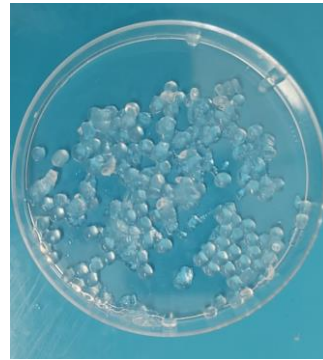


Figure S3. Photographs of chitosan and calcium–alginate hydrogel beads before and after adsorption of syringic acid

Figure S3a. Photographs of calcium–alginate hydrogel beads before and after adsorption of syringic acid.



Before



After

Alginate beads are damaged after adsorption

Figure S3b. Photographs of chitosan hydrogel beads before and after adsorption of syringic acid



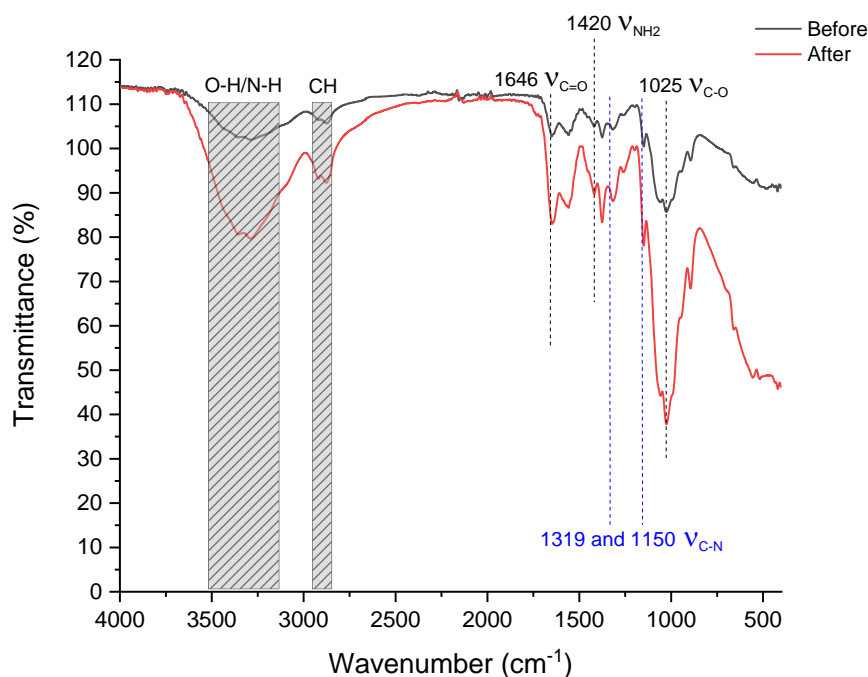
Before



After

The used beads seem to be unaffected after adsorption

Figure S4. FTIR spectra of chitosan hydrogel beads before and after syringic adsorption.



FTIR spectra of chitosan hydrogels before and after adsorption of syringic acid was undertaken (Figure S4). Before adsorption, some characteristic bands of chitosan can be depicted.

For example the broad band ranging from 3200 to 3500 cm^{-1} is due to the overlap of the stretching vibration bands of O-H and N-H, while those at 2875, 1646, 1420 and 1375 cm^{-1} correspond to -CH stretching vibration in -CH and -CH₂, C=O stretching of amide I, -NH deformation vibration in -NH₂ and -CH symmetric bending vibration in -CHOH- respectively. The bands situated at 1319 and 1150 cm^{-1} can be assigned to C-N stretching vibration, and the ones at 1061 and 1025 cm^{-1} refer to C-O stretching vibration in C-OH, respectively. After adsorption, an increase in the peaks intensity of OH, C=O and C-O band region can be easily observed, which may result from additional syringic acid hydroxyl and carboxyl functional groups. However, no additional new band can be depicted, probably because of the extent of hydrogen bonding in the hydrogel network that causes signal and broadening and consequently do not allow for discriminating the fingerprint of the adsorbed syringic acid.

Figure S5. Adsorption kinetics and performance after 3 h and 24 h of contact of chitosan and chitosan-filled beads toward syringic acid.

Figure S5a. Adsorption kinetics of syringic acid over time using chitosan and chitosan-filled beads

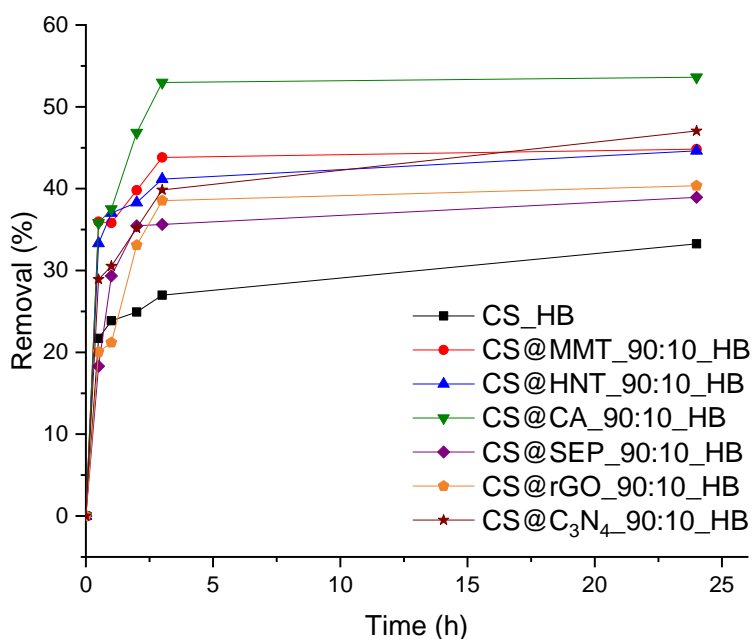


Figure S5b. Adsorption performance of chitosan and chitosan-filled beads after 3 h and 24 h of contact.

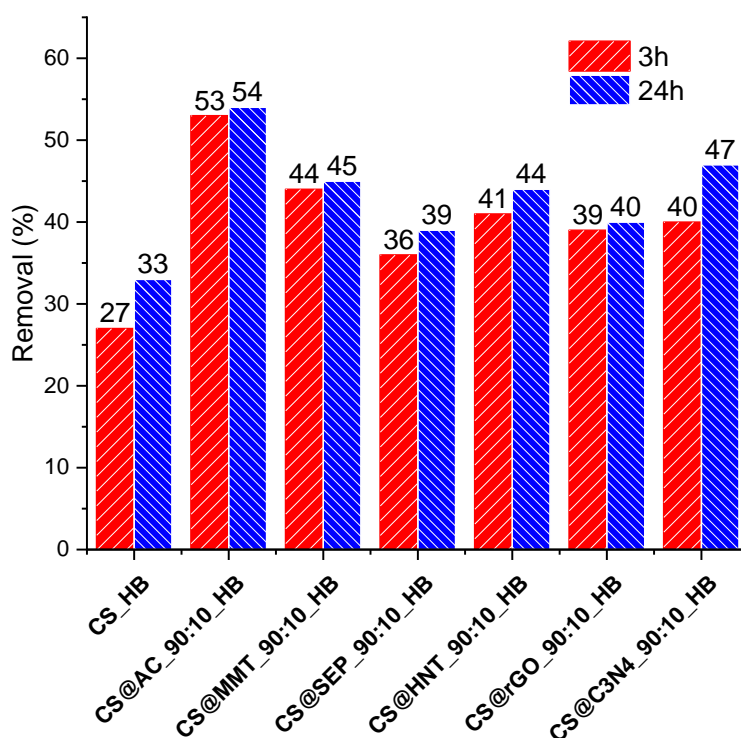


Figure S6. Schematic illustration of the structural arrangements of layered nanosheets within polymer matrices as a function of the filler content: agglomeration, intercalation and exfoliation.

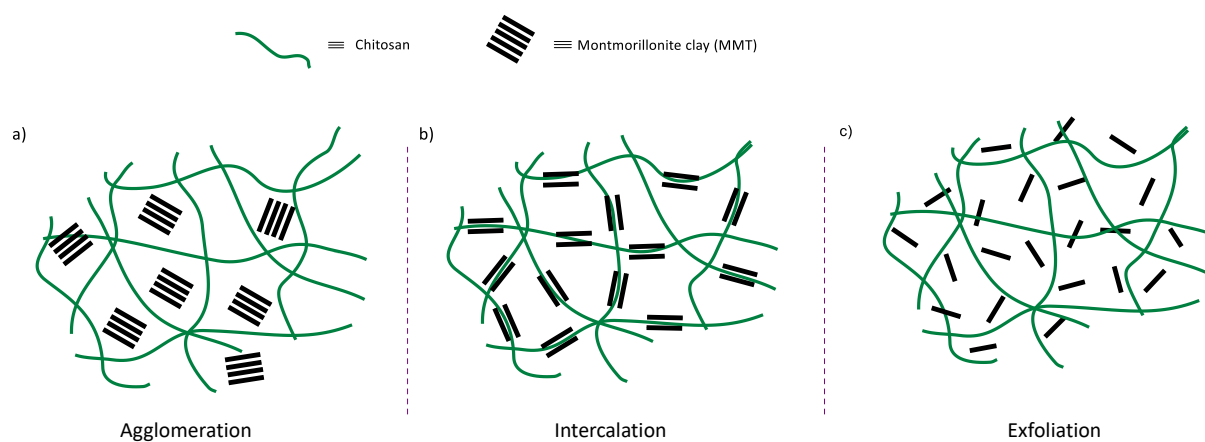
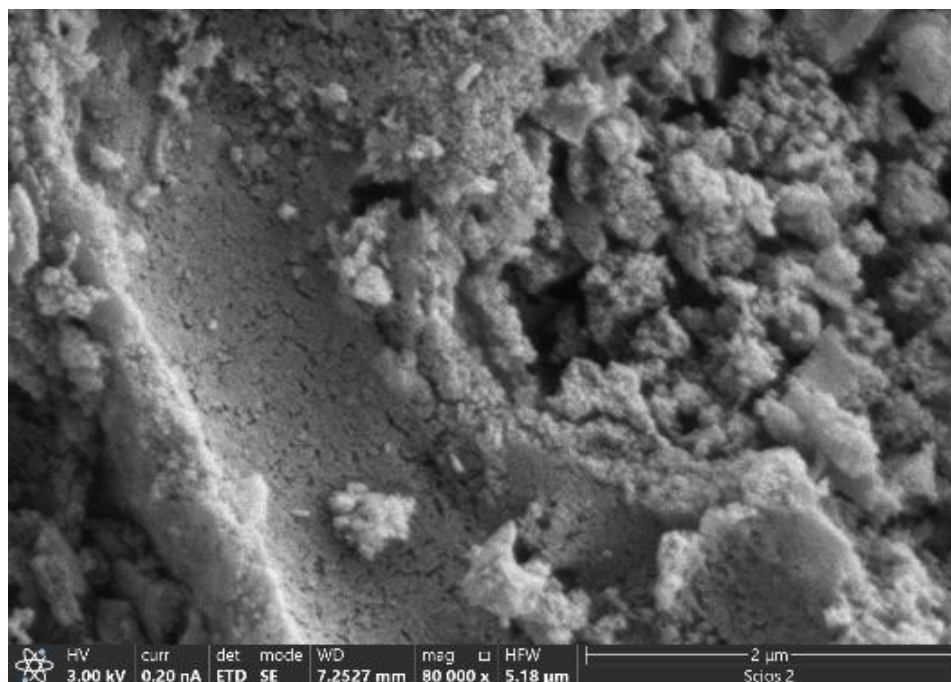
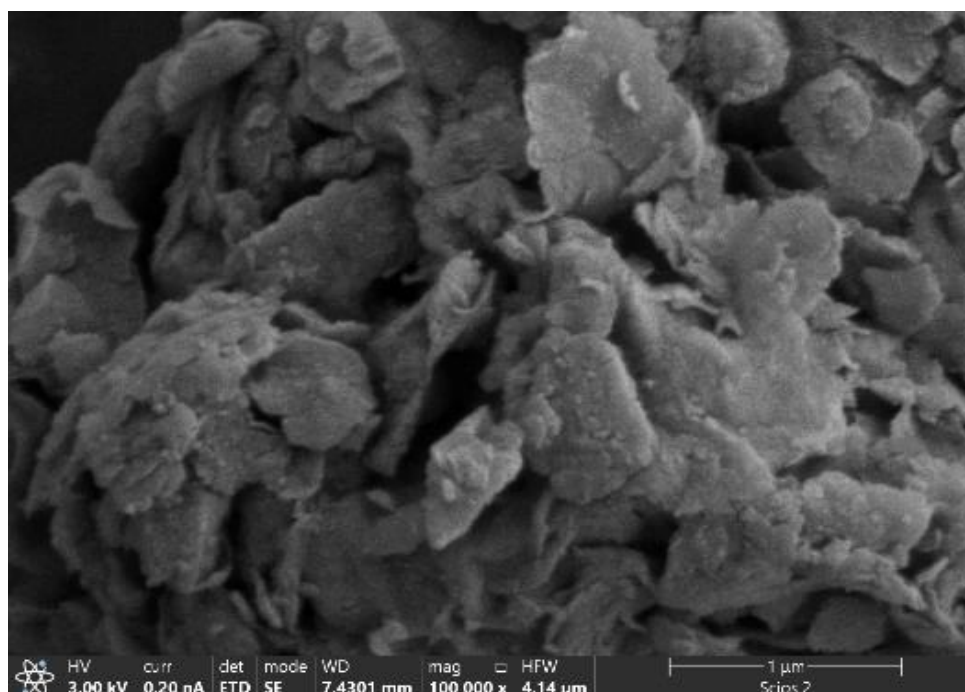


Figure S7. SEM of activated carbon (AC) and montmorillonite (MMT).



SEM of active carbon



SEM of MMT

Table S1. Textural properties of the investigated materials.

Sample	Specific surface area $\text{m}^2.\text{g}^{-1}$	Pore Volume $(\text{cm}^3.\text{g}^{-1})$	Pore diameter (nm)
CS_CB	21.3	0.06	26.9
CS_XB	0.05	0.006	57.4
AC	764.3	0.4	6.9
MMT	281.2	0.5	6.6
CS@MMT_50 :50_CB	16.2	0.05	15
CS@MMT_50:50_XB	1.8	0.004	9.4
CS@AC_50 :50_CB	310.2	0.2	11.1
CS@AC_50:50_XB	248.1	0.6	15.2

Table S2. Residual mass (%) of adsorbents at selected temperatures from TGA analysis.

Sample	Residual mass at 100 °C (%)	Residual mass at 320 °C (%)	Residual mass at 700 °C (%)
CS_XB	98	57	18
AC	89	40	40
MMT	90	88	85
CS@AC_50:50_XB	96	73	27
CS@MMT_50:50_XB	99	76	48

Figure S8. Comparative views of **CS@MMT_50:50_HB** and **CS@AC_50:50_HB** beads before and after adsorption of caffeic and syringic acids

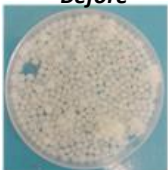

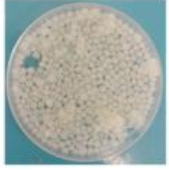

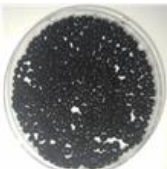
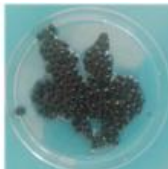
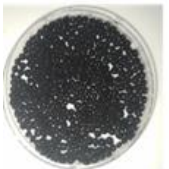
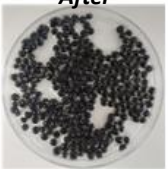
<div>Adsorbate</div> <div>Adsorbent</div>	<div> <chem>O=C(O)/C=C/c1ccc(O)c(O)c1</chem> Caffeic acid </div>	<div> <chem>O=C(O)c1cc(OC)c(OC)c(O)c1</chem> Syringic acid </div>
CS@MMT_50:50_HB	<div>Before</div>  <div>After</div> 	<div>Before</div>  <div>After</div> 
CS@AC_50:50_HB	<div>Before</div>  <div>After</div> 	<div>Before</div>  <div>After</div> 

Figure S9. DRFIT spectra of **CS@AC_50:50_HB** before and after adsorption of syringic acid and caffeic acid.

Figure S9a. DRFIT spectra of **CS@AC_50:50_HB** before and after adsorption of syringic acid

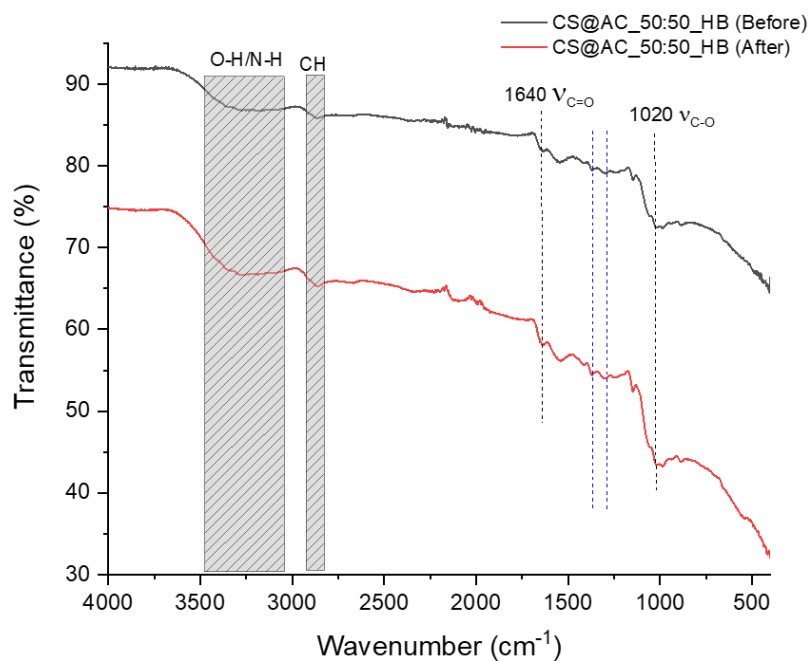


Figure S9b. DRFIT spectra of **CS@AC_50:50_HB** before and after adsorption of caffeic acid.

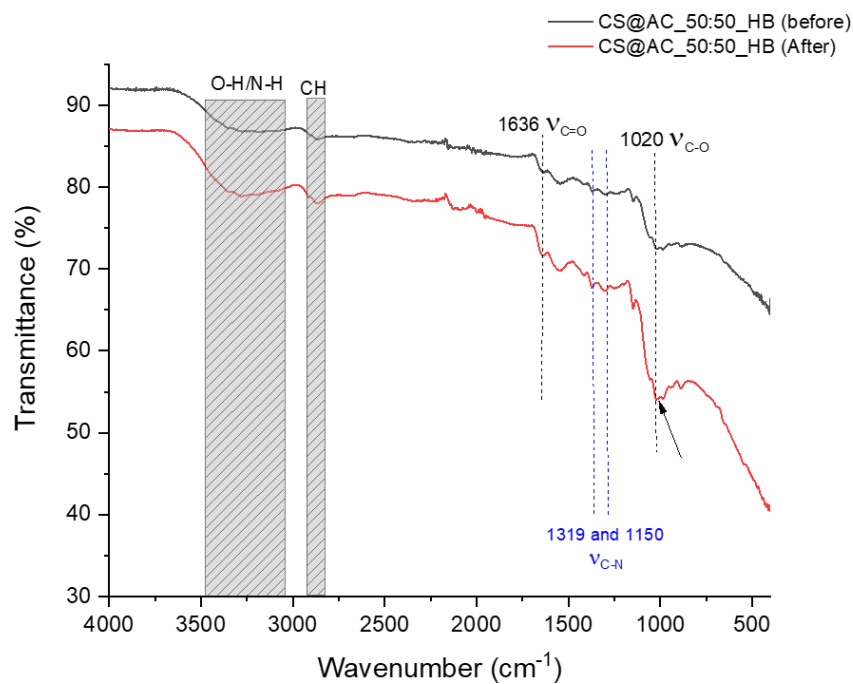


Table S3. Physicochemical parameters of raw, diluted, and treated Olive Mill Wastewater (OMW) using chitosan and chitosan-filled beads

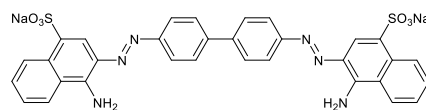
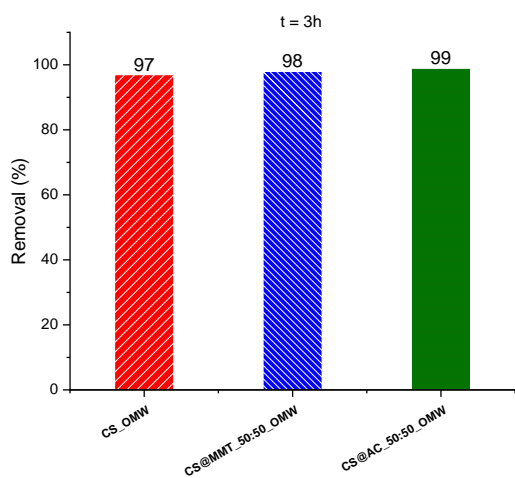
Table S3a. Physicochemical parameters of raw, diluted Olive Mill Wastewater (OMW)

Sample	pH	COD (mgO ₂ /l)	BOD ₅ (mg O ₂ /l)	Turbidity (NTU)	Conductivity (μs/cm)	TDS (mg/l)	Salinity (mg/l)
Raw OMW	4.47	128408.5	12500	36950	7678	47723	4200
OMW 1/100	6.2	1284.1	125	355	81.8	476	5

Table S3b. Physicochemical Parameters of Treated Olive Mill Wastewater (OMW) Using chitosan and Chitosan-Filled Beads

Chitosan-Filled Beads	pH	COD (mgO ₂ /l)	BOD ₅ (mg O ₂ /l)	Turbidity (NTU)	Conductivity (μs/cm)	TDS (mg/l)	Salinity (mg/l)
CS_HB	6.4	17.52	542	6.68	32.3	13	0
CS@MMT_50:50_HB	6.2	35.88	424	1.91	18.9	9	0
CS@AC_50:50_HB	6.1	8.52	288	1.71	17.4	7	0

Figure S10. Adsorption performance of OMW-saturated chitosan and chitosan-filled beads Toward Congo Red, Tetracycline, and Copper(II) Ions



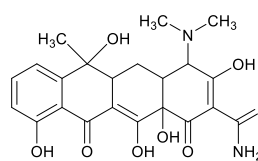
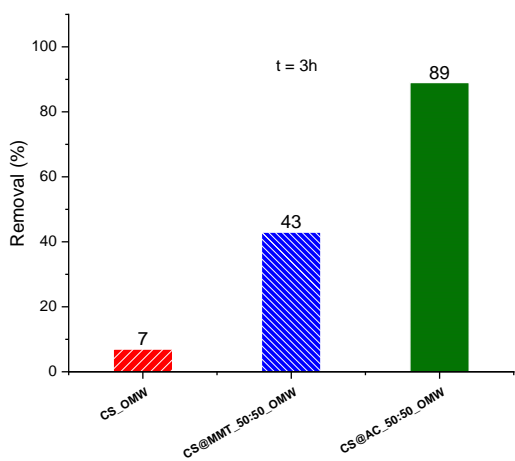
CS_OMW



CS@MMT_50:50_OMW



CS@AC_50:50_OMW



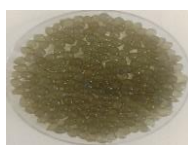
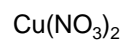
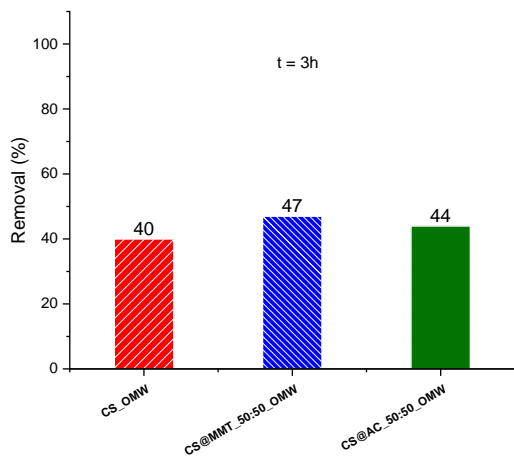
CS_OMW



CS@MMT_50:50_OMW



CS@AC_50:50_OMW



CS_OMW



CS@MMT_50:50_OMW



CS@AC_50:50_OMW